More than three-fold increase of compound soil and air dryness across Europe by end of 21st century

Ankit Shekhar
ankit.shekhar@usys.ethz.ch

ETH Zurich https://orcid.org/0000-0003-0802-2821

Vincent Humphrey
Federal Office of Meteorology and Climate MeteoSwiss

Nina Buchmann
ETH Zurich https://orcid.org/0000-0003-0826-2980

Mana Gharun
ETH Zürich https://orcid.org/0000-0003-0337-7367

Research Article

Keywords:

Posted Date: August 16th, 2023

DOI: https://doi.org/10.21203/rs.3.rs-3143908/v2

Additional Declarations: There is **NO** Competing Interest.

Version of Record: A version of this preprint was published at Weather and Climate Extremes on March 1st, 2024. See the published version at https://doi.org/10.1016/j.wace.2024.100666.

More than three-fold increase of compound soil and air dryness across Europe by end of 21st century

Ankit Shekhar[1], Nina Buchmann[1], Vincent Humphrey[2] Mana Gharun[3]

[1] Department of Environmental Systems Science, ETH Zürich, 8092 Zürich, Switzerland

[2] Federal Office of Meteorology and Climate MeteoSwiss, Zürich, Switzerland

[3] Faculty of Geosciences, University of Münster, 48149 Münster, Germany

Abstract

Increases in air temperature leads to increased dryness of the air and potentially develops increased dryness in the soil. Extreme dryness (in the soil and/or in the atmosphere) affects the capacity of ecosystems for functioning and for modulating the climate for example through CO_2 uptake or evaporative cooling. Here, we used daily soil moisture and vapor pressure deficit data of high spatial resolution (~ 0.1° × 0.1°) from 1950-2100 to show that compared to the reference period (1950-1990), the frequency and intensity of extreme soil dryness, extreme air dryness, and compound extreme dryness (i.e., co-occurrence of extreme soil and air dryness) has increased over last 31 years (1991-2021) and will further continue to increase in the future until 2100 across Europe. This increased intensity and frequency was most pronounced over broadleaved forests, croplands, and grasslands. Such future climate-change induced increase in extreme dry conditions could alter ecosystem functioning across Europe.

Introduction

Our Earth has been experiencing an unprecedented rate of warming since the start of the 20th century. According to a report from “Copernicus Climate Indicators”, global mean air temperature has increased by 1.2°C since the pre-industrial period of 1850-1900, whereas surface air temperature over Europe has increased by 2.2°C (https://climate.copernicus.eu/climate-indicators/temperature). In the absence of additional precipitation, warming over land leads to increased air dryness (measured by vapor pressure deficit, VPD) which can lead to increased evapotranspiration (ET) and a faster soil drying[1,2]. In addition, low precipitation will lead to low soil moisture (SM) if ET draws down available soil water pools. If both conditions co-occur, i.e., high VPD and low SM, a compound dry conditions, or even compound extreme dryness develop, i.e., co-occurrence of extreme high VPD values (e.g., VPD > 90th percentile; extreme air dryness) and extreme low SM levels (e.g., SM < 10th percentile; extreme soil dryness)[3,4].

High VPD and low SM have been recognized as two constraints on the water use and carbon uptake by terrestrial ecosystems[5–9]. Plants typically decrease their stomatal conductance in response to high VPD and low SM to limit water loss and prevent hydraulic failure[10] thereby also reducing photosynthesis rates and thus CO_2 uptake. Even though high VPD and low SM conditions are known to frequently occur simultaneously[11], their impacts on vegetation are often assessed independently[12]. This tendency for co-occurrence of high VPD and low SM conditions could cause a larger heat- and drought-driven decrease in net CO_2 uptake by vegetation compared to conditions when VPD and soil dryness do not become limiting at the same time. Therefore, it is crucial to assess how VPD and SM are coupled, especially in regard to the co-occurrence of extreme high VPD and extreme low SM conditions (i.e., compound extreme dryness).

Although over the past 40 years, most parts of Europe have experienced persistent precipitation patterns[13]. At the same time increased air temperature (and thus increased VPD) driven increasing ET might have resulted in soil drying trends, however the causation is difficult to establish[13]. Thus, the impact of global warming has had profound devastating effects on Europe´s land ecosystems, especially in the 21st century when it was impacted by drought and heat waves in 2003, 2010, 2015, 2018, 2019 and the most recent in 2022[14–17]. With both soil drying and air drying trends, frequency and intensity of compound extreme dryness in Europe are largely bound to increase especially during the main carbon uptake period (April-September) when the terrestrial ecosystem acts as a sink[18]. Furthermore, this trend in soil and air drying could increase the SM and VPD covariance (coupling) which will further increase the frequency of compound extreme dryness along with decreased SM and increased VPD trends in the future[12,19]. A previous study[12] highlighted the increase in frequency of compound air and soil dryness globally using data from earth system models (ESMs) at monthly timescale. However, it is known that carbon and water fluxes of terrestrial ecosystems shows immediate response to variation in weather, particularly at daily time scales. Eddy covariance measurements that are used to measure ecosystem carbon fluxes, because of their high temporal resolution (half-hourly), have shown such short-term response of ecosystems to climate extremes[20–23]. Furthermore, high-resolution tree growth measurements collected with dendrometers show that extreme atmospheric dryness and low soil moisture conditions affect tree growth on the daily and even sub-daily time scale[24]. Therefore, assessing the evolution of extreme SM and VPD at daily timescale would be relevant for assessing its impact on ecosystem functioning. Additionally, little is known about how trends in daily SM and VPD and its coupling have changed the intensity and frequency of these compound extreme dryness over the past decades and how they are projected to change in the future.

In this study we aim (i) to quantify how intensity and frequency of occurrences of extreme soil dryness, extreme air dryness and compound extreme dryness i.e., co-occurring extreme soil dryness AND extreme air dryness (collectively as extreme dryness) have changed across Europe since the 1950s, and how they are projected to change in the future until 2100; (ii) to quantify the changes in SM and VPD coupling and its impact on compound extreme dryness across Europe from 1950 to 2100. To achieve these objectives, we use high-resolution (0.1°× 0.1°) daily in-situ observation based VPD (calculated from air temperature and relative humidity as daily average) from E-OBS[25] and SM from ERA5-Land reanalysis data[26] from 1950-2021. For future projections of extreme dryness, we used historical and future climatic projection (1950-2100) data of daily VPD and SM from EURO-CORDEX[27] simulations (0.11° × 0.11°) over the European continent (comprising of three distinct regions, namely Northern Europe (NEU), Central Europe (CEU) and Mediterranean Europe (MED) as shown in Figure S1a[17]). We used EURO-CORDEX simulations from five RCMs (Regional Climatic Models) driven under the RCP8.5 (Representative Concentration Pathways 8.5) emission scenario. We also segregate the changes quantified in (i) and (ii) across different land cover types based on 2021 MODIS land cover data[28] (MCD12Q1 version 6.1) as shown in Figure S1b to highlight changes in intensity and frequency of extreme dryness of the present land cover of Europe.

The novelty of our study is in using a higher spatial (0.1° x 0.1°) and temporal (daily) resolution in the analysis of soil and air dryness, and characterizing their extremes based on the recently-developed notion from high resolution environmental observations, that these extremes are particularly relevant for ecosystem functioning at shorter time scales[21,22]. Since extreme dryness is relevant for terrestrial carbon cycle, we focused all our analyses during the April-September months (183 days) as most of the carbon sink activity occurs during this period across Europe[18]. We assumed 1950-1990 as a reference period (total 41×183 = 7503 days) and 1991-2021 as the present period (total 5673 days). We divided the future period into two slices of 35 years each: 2031-2065 (mid 21st century; 6405 days) and 2066-2100 (late 21st century; 6405 days) to quantify and compare the intensity and frequency of each type of extreme dryness. We used the "peak over threshold" approach to identify extreme soil dryness ($SM < SM_{10P}$; 10^{th} percentile SM), extreme air dryness ($VPD > VPD_{90P}$; 90^{th} percentile VPD) and compound extreme dryness days ($SM < SM_{10P}$ AND $VPD > VPD_{90P}$) across Europe during each of the reference, present and future periods[4,12]. The intensity of extremes was defined by the extreme SM and VPD thresholds, i.e., SM_{10P} and VPD_{90P}, for reference, present and future periods. Decrease in SM_{10P} (across different periods) implied increased intensity of extreme soil dryness, whereas increase in VPD_{90P} implied increased intensity of extreme air dryness and vice-versa.

Results

A drying Europe

The majority of Central Europe (CEU) and Mediterranean Europe (MED) showed a significant negative trend in the yearly mean soil moisture (SM) in the topsoil (0-7 cm; April to September), while Northern Europe (NEU) has showed substantial soil wetting as indicated by the positive trend in SM (Figure 1a) from 1950-2021. Except for southwestern Finland, yearly mean VPD (April to September) showed a significantly increasing trend between 1950 and 2021, with parts of southern Spain showed the highest positive trend of more than 0.1 kPa/decade (Figure 1c). Additionally, we also explored the trends of the yearly extreme thresholds of SM and VPD, i.e., yearly SM_{10P} (10^{th} percentile SM of each year) and VPD_{90P} (90^{th} percentile VPD of each year). The patterns of yearly SM_{10P} and VPD_{90P} trends (Figure 1b & 1d) were spatially similar but more pronounced than those of the yearly mean SM and VPD trends (Figure 1a & 1c). The trends of SM_{10P} and VPD_{90P} were about 35% and 80% higher than those of yearly mean SM and VPD between 1950 and 2021, respectively (indicated by slope of the linear regression in Figure S2). This indicated that the rate of intensification of extreme soil and air drying was higher than that mean drying. Therefore, we observed development of compound dry conditions characterized by both decreasing trend of SM and increasing trend of VPD across most of the CEU and MED over last 72 years (1950-2021).

Changes in extreme soil dryness and air dryness

Compared to the reference period, the SM_{10P} threshold (indication of intensity of extreme soil dryness) of the present period in CEU and MED was typically 15% to 25% lower (i.e., intensity of extreme soil dryness increased by 15 to 25 %). In contrast, the SM_{10P} in NEU was about 10% higher than that during the reference period (Figure 2a), implying a 10% decrease in intensity of extreme soil dryness. The spatial pattern of change in frequency was similar to that of change in intensity of extreme soil dryness (Figure 2a, b). The frequency of extreme soil dryness increased 1.2-fold[0.8,1.6] (median[10^{th} , 90^{th} percentile] (Figure 2b) across Europe (compared to the reference), with most of CEU and MED showed more than a 1.5-fold increase in frequency of extreme soil dryness. Both increased in intensity and frequency of extreme soil dryness was prominent for urban areas, croplands, as well as broadleaved and mixed forests (Figure 2c, d).

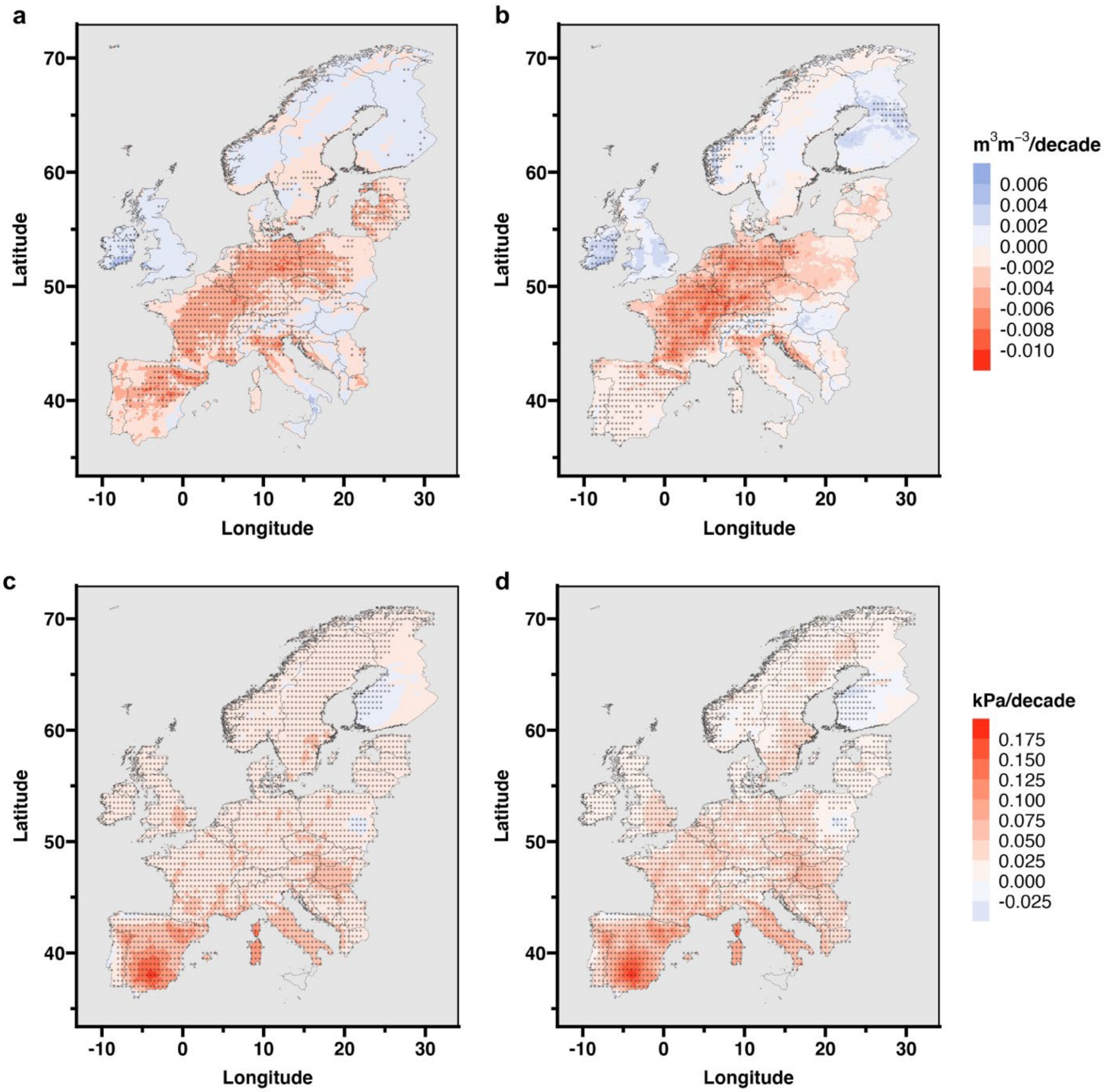

Figure 1. Pronounced soil drying **(a, b)** and air drying **(c ,d)** of Europe during the months April to September between 1950 and 2021 as demonstrated by negative trends of (a) yearly mean soil moisture, and (b) yearly 10th percentile soil moisture (SM10P), and positive trends of (c) yearly mean VPD, and (d) yearly 90th percentile VPD (VPD90P). The significant trend ($p<0.05$) areas are marked by black dots based on a modified Mann-Kendall trend test (see Methods).

Except for Finland, the VPD_{90P} threshold (indication of intensity of extreme air dryness) of the present period was higher than that of the reference period across Europe (Figure 3a). Overall, the increase in intensity of extreme air dryness across Europe was about 15%, with more than 50% increase in intensity for majority of MED. The spatial pattern of change in frequency was similar to that of change in intensity of extreme air dryness (Figure 3a, b). The frequency of extreme air dryness largely increased across Europe (compared to the reference), with about 1.6-fold [1,2.3] increase (median[10^{th} , 90^{th} percentile] over Europe (Figure 3b) and about one-quarter of Europe showing more than a two-fold increase in frequency of extreme air dryness during the present period in comparison to the reference period. Both increased in intensity and frequency of extreme air dryness was prominent (intensity > 20% and frequency > two-fold) for urban areas, croplands, as well as broadleaved forests (Figure 3c, d).

Daily SM-VPD coupling

Compound extreme dryness, i.e., the co-occurrence of extreme soil and air dryness not only relate to changes in either SM and VPD contributing to the compound extreme, but also to the relationship between SM and VPD. Daily topsoil SM and VPD values were significantly negatively correlated, indicating strong (negative) SM-VPD coupling across most of Europe during the reference and the present period (Figure S3). Weak SM-VPD coupling [absolute r(SM,VPD) < 0.2] was observed at higher latitudes (> 65°N), particularly at higher elevations (NEU), and in the Alpine region (CEU; Figure S3a,b). Compared to the reference period (median r(SM,VPD) of -0.55), the present period showed a stronger SM-VPD coupling dependence (median r(SM,VPD) of -0.61), with more than 80% of Europe showing stronger SM-VPD coupling, largely consistent across land cover types (Figure 4). This increase in strength of SM-VPD coupling during the present period was highest in NEU and the Alpine region of CEU (Figure 4). Furthermore, overall, the daily SM-VPD coupling was significantly lower than monthly SM-VPD coupling (Figure S4a) as also observed in previous studies but there were regional differences.

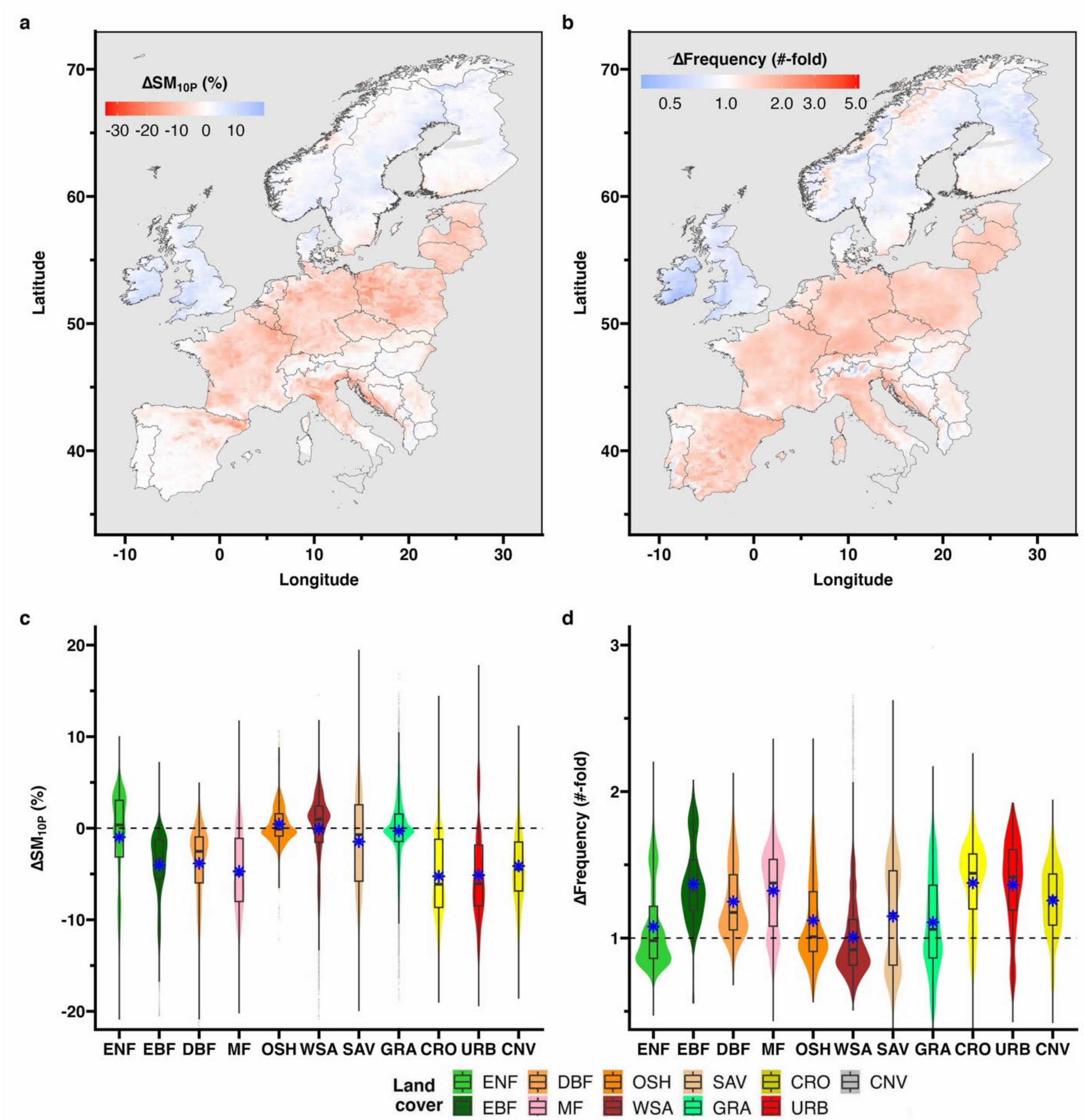

Figure 2. Change in intensity (as indicated by SM_{10P}) **(a, c)** and frequency **(b, d)** of extreme soil dryness across Europe and land cover types during the present period (1991-2021) in comparison to the reference period (1950-1990). The change in intensity is calculated as % change in the present period compared to the reference period of SM_{10P} (10th percentile of SM) indicated as ΔSM_{10P} (100 × (present–reference)/reference). The change in frequency of occurrences (ΔFrequency) is shown in terms of n-fold (present/reference). The blue asterisks in c and d shows the means. The land cover types were based on the IGBP land cover classification (see Methods or caption of Figure S1).

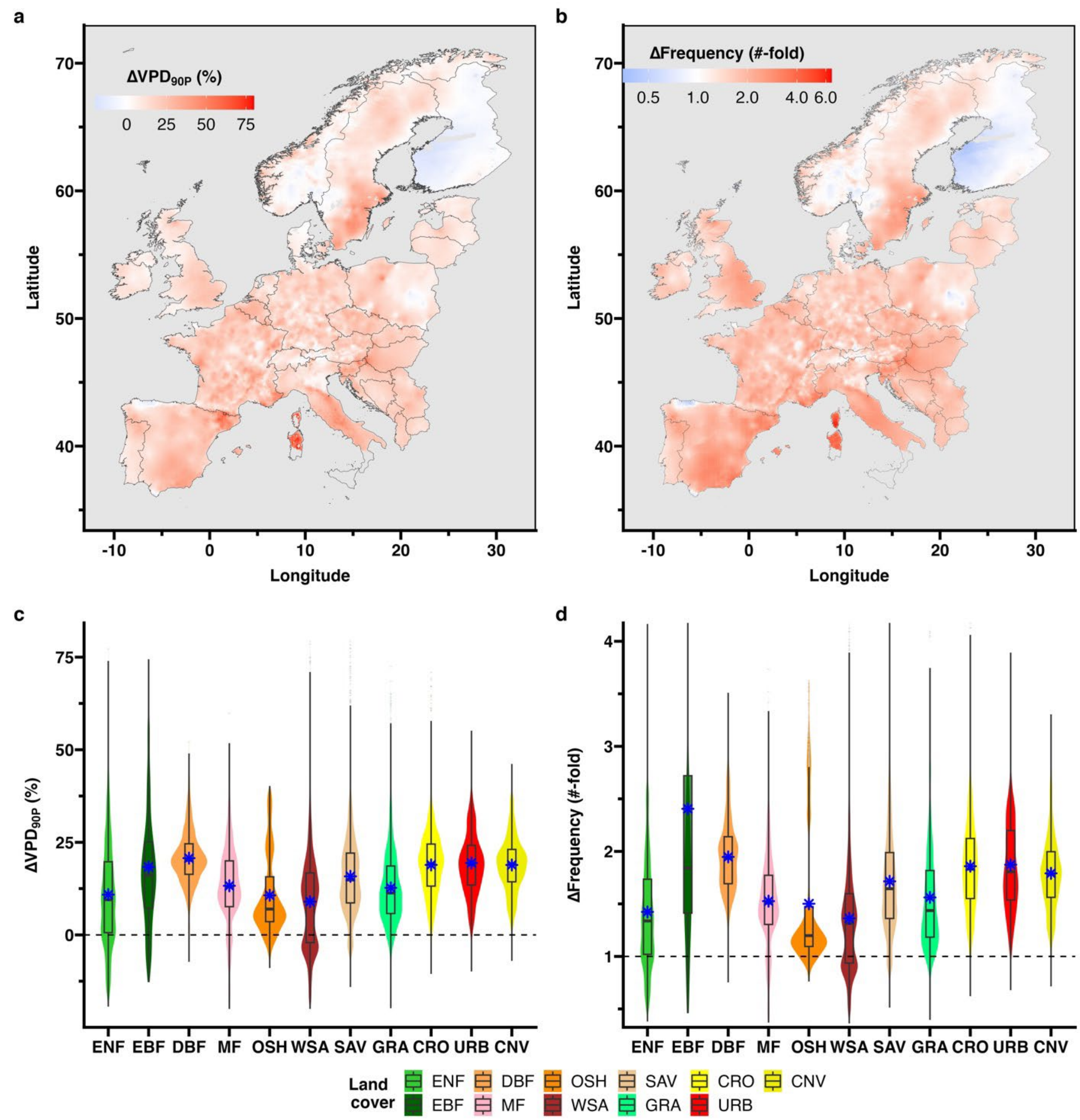

Figure 3. Change in intensity (as indicated by VPD_{90P}) **(a, c)** and frequency **(b, d)** of extreme air dryness across Europe and land cover types during the present period (1991-2021) in comparison to the reference period (1950-1990). The change in intensity is calculated as % change in the present period compared to the reference period of VPD_{90P} (90th percentile of VPD) indicated as ΔVPD_{90P} ($100 \times$ (present–reference)/reference). The change in frequency of occurrences (ΔFrequency) is shown in terms of n-fold (present/reference). The blue asterisks in c and d shows the means. The land cover types were based on the IGBP land cover classification (see Methods or caption of Figure S1).

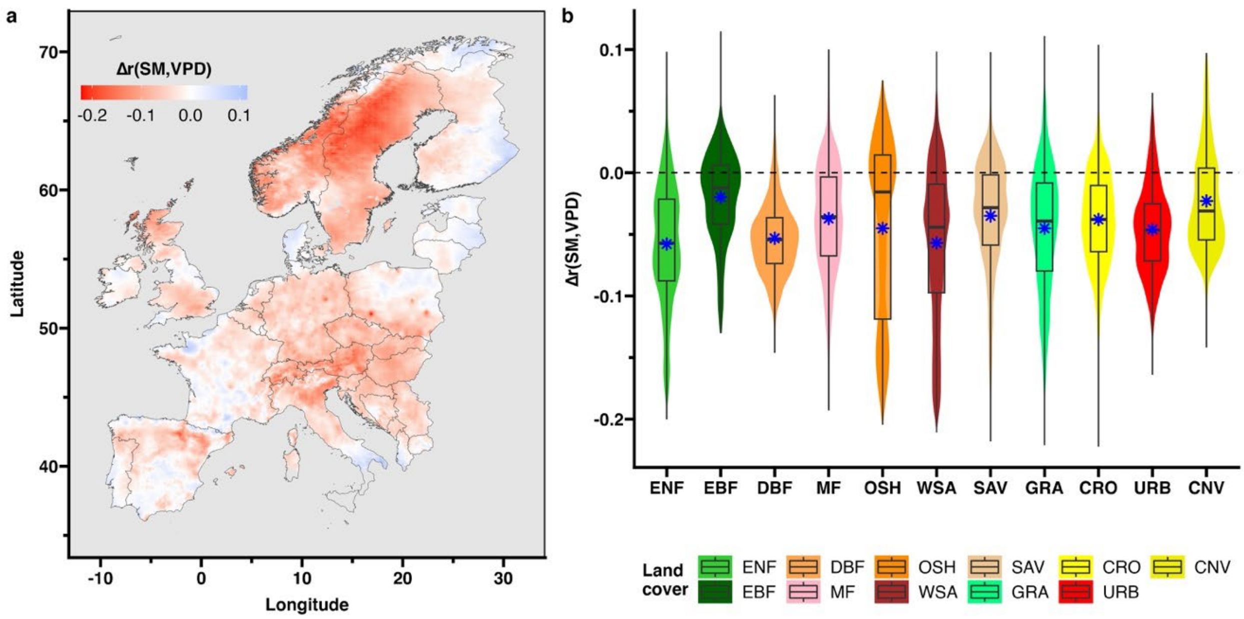

Figure 4. Change in negative coupling (present-reference) between daily topsoil SM and VPD as indicated by change in Pearson correlation coefficient [Δr(SM,VPD)] between present and reference period **(a)** across Europe and **(b)** land cover types. The blue asterisk in b shows the means. The land cover types were based on the IGBP land cover classification (see Methods or caption of Figure S1).

To quantify the impact on daily SM-VPD coupling on the frequency of occurrence of compound extreme dryness, we calculated the probability multiplication factor (PMF). The PMF indicated the increased probability (or frequency of occurrence) of compound extreme dryness compared to that expected when SM and VPD are independent (i.e., P = 0.1 × 0.1 = 0.01; see Methods). The PMF across Europe during the reference period was 3.6 [2.5, 4.2] (median [10^{th} percentile, 90^{th} percentile]), indicating that the frequency of co-occurrence of soil and air dryness (i.e., compound extreme dryness) during the reference period was 3.6 time more than if SM and VPD would have been independent (Figure S5a). As expected, due to increased SM-VPD coupling over large parts of Europe (Figure 4), the PMF during the present period increased to 4 [2.9, 4.6] across Europe (Figure S5b). This increase in present day PMF compared to the reference PMF was largest over NEU, Alpine region, and southern Spain (more than 1.5-fold; Figure 5a). However, across France and southern Italy, the PMF decreased during the present period (Figure 5a). Among different land cover types, the highest observed increase in PMF was over shrublands and grasslands (mean of 1.2-fold; Figure 5b). The relationship between daily SM and VPD coupling, as indicated by r(SM, VPD), and PMF for compound extreme dryness was largely linear, with an increase of PMF with increase in negative coupling in CEU and NEU (Figure 6). However, in MED, we observed a decrease in PMF for r(SM, VPD) < -0.6 as shown in Figure 6. Furthermore, the relationship between PMF and r(SM, VPD) was significantly different between reference and present period over MED (for r(SM, VPD) < -0.6) and NEU (for r(SM, VPD) < -0.2), with higher PMF values during the present period compared to reference period (Figure 6). However, across CEU, the PMF vs r(SM, VPD) relationship remained unchanged during present and reference period (Figure 6). Additionally, similar to the SM-VPD coupling, overall, the PMF at daily timescale was significantly lower than PMF at monthly timescale (Figure S4b), indicating overestimation of frequency of compound extreme dryness at monthly timescales in comparison to daily timescales.

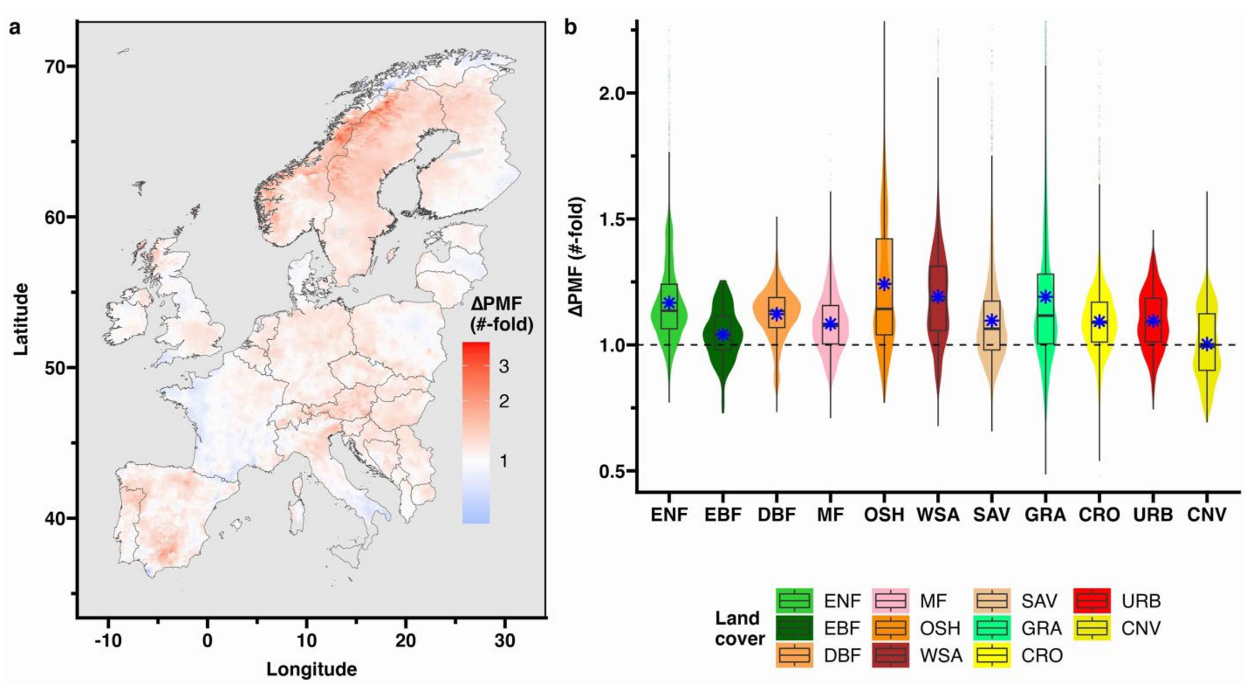

Figure 5. Change in probability multiplication factor (PMF) of compound extreme dryness during as (a) number of fold (ΔPMF; present/reference) across Europe and its **(b)** segregation across different land cover types. The blue asterisk in panel d shows the means. The land cover types are based on the IGBP land cover classification (see Methods or caption of Figure S1).

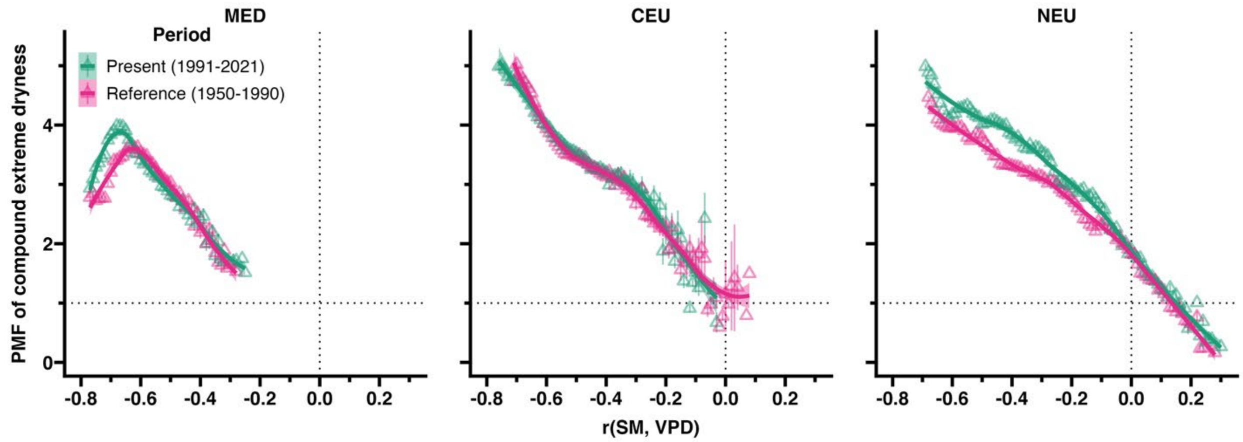

Figure 6. Relationship of coefficient correlation between daily SM and VPD (x-axis: r(SM,VPD) with probability multiplication factor of compound extreme dryness across Mediterranean Europe (MED), Central Europe (CEU) and Northern Europe (NEU) during reference period (1950-1990) and present period (1991-2021). The curve fitting is done with a locally moving weighted regression (loess with span = 0.8). Each point and error bar represents mean and standard error for a bin of r(SM,VPD) = 0.01.

Change in frequency of compound extreme dryness

The probability of the occurrence, which indicates frequency, of compound extreme dryness (P_{CD}) across Europe during the reference period is also equal to the PMF of the reference period, i.e., 3.5±0.7 % (mean±sd) as shown in Figure 7a. Using the SM_{10P} and VPD_{90P} thresholds from the reference period, the P_{CD} increased to 6.0±2.4% during the present period (Figure 7b), thereby showing a 1.7-fold [0.9,2.5] (median[10^{th}, 90^{th} percentile]) increase overall across Europe and more than 2-fold increase for more than one-quarter of the European land area (Figure 7c). The increase in P_{CD} was highest in the MED (more than 4-fold increase), whereas a decrease in occurrence was observed in some areas of NEU (i.e., Finland, Ireland, and the western part of the UK), comprising about 12% of the study area (Figure 7c). To understand if this increase in P_{CD} was due to increase in SM-VPD coupling or due to decreasing SM and/or increasing VPD trend from reference to present period, we calculated ΔP_{CD} due to SM-VPD coupling (ratio of PMF in present and reference period) and due to SM and VPD trend (ratio of P_{CD} and PMF of reference period; see Methods). Our results indicate that the increase in P_{CD} across CEU (excluding the Alpine area) and MED was dominantly due to the decreasing SM and/or increasing VPD trend from reference to the present period (Figure 8a). Whereas, for much of the NEU and Alpine region in CEU, the ΔP_{CD} was due to the increased SM-VPD from reference to the present period. Overall, the change in SM-VPD coupling (as shown in Figures 4 & 5) resulted in a ΔP_{CD} of 1.1-fold [0.9,1.4], whereas decreasing SM and/or increasing VPD trend resulted in a ΔP_{CD} of 1.5-fold [0.9, 2.3] (Figures S6 & 8b). Among different land cover types, we observed a mean increase in the frequency by more than 2-fold over evergreen broadleaved forests, croplands, and urban areas during the present period in comparison to the reference period (Figure 7d).

Future projections of compound extreme dryness

Climate projections indicated a further compound drying (both soil and air drying) trend across Europe. Compared to the reference period, the decrease in average SM_{10P} across Europe was only marginal, i.e., 1%, 3% and 3.5% decrease during the present period, mid 21st century (2030-2065), and late 21st century (2066-2100), respectively (Figure S7a) with largest decrease in MED (Figure S8a). The VPD_{90P} however showed an average increase across Europe by 12%, 35% and 68% compared to the reference period, during the present period, mid 21st century, and late 21st century, respectively, as simulated by the five RCMs (Figure S7b), with largest increase in CEU (Figure S8b). Furthermore, the ensemble means value (mean from all five RCMs) of the Pearson coefficient correlation – r(SM, VPD) indicated a significantly increasing SM-VPD from 1950-2100 (larger negative correlations from reference to future periods; Figure S9). The RCM models, however, underestimated the SM-VPD coupling as the mean correlation coefficient during reference and present period obtained from RCM models were -0.33 and -0.35 (Figure S9), significantly lower than the correlation coefficient obtained from E-OBS and ERA5-Land data (-0.5 and -0.54 during reference and present periods, respectively as shown in Figure S3). Furthermore, the increase in SM-VPD coupling simulated by the RCMs did not significantly increase the PMF of compound extreme dryness across MED, CEU, and NEU (Figure S10).

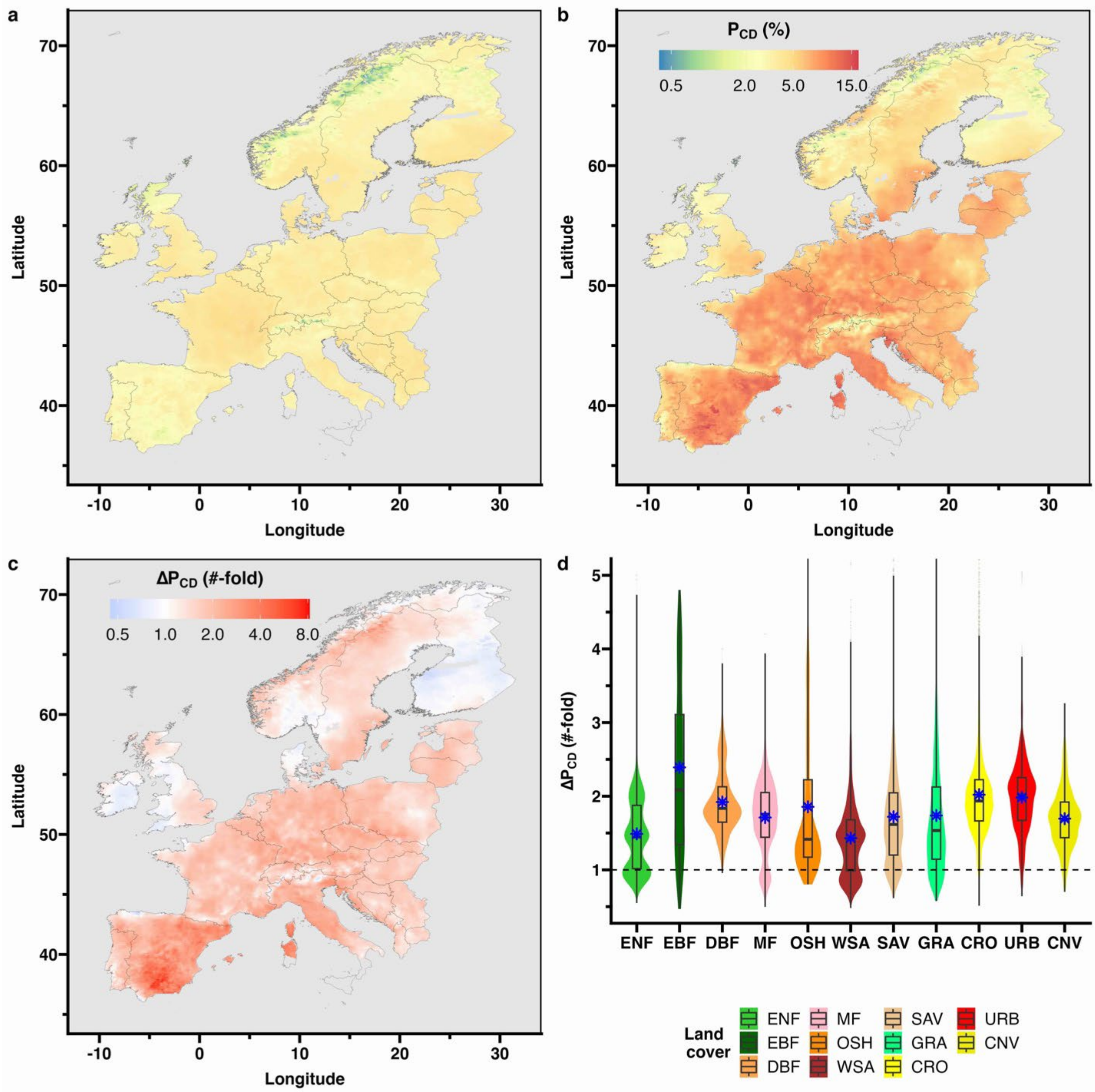

Figure 7. Probability of the occurrence indicating frequency of compound extreme dryness (P_{CD}) during **(a)** the reference period, **(b)** the present period (with SM and VPD thresholds from reference period), **(c)** change in probability of compound extreme dryness (ΔP_{CD}) between present and reference period (ΔP_{CD} = present/reference), and **(d)** the change across different land cover types. The blue asterisk in panel d shows the means. The land cover types are based on the IGBP land cover classification (see Methods or caption of Figure S1).

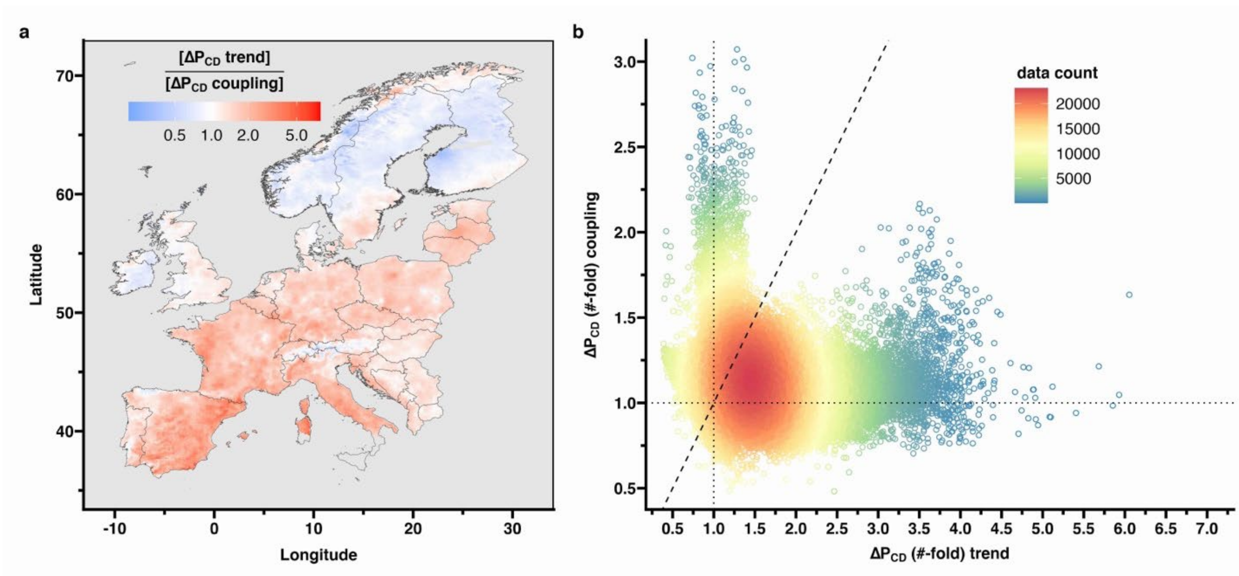

Figure 8. (a) Ratio of change in probability of occurrence of compound extreme dryness between present and reference period (ΔP_{CD} = present/reference) due to SM and VPD trend and SM-VPD coupling across Europe and (b) comparison of the ΔP_{CD} due to trend of SM and VPD (x-axis) and SM-VPD coupling (y-axis) for all locations in Europe. Values lower than one in panel a and above the 1:1 line in panel b indicate that SM-VPD coupling was the dominant reason for ΔP_{CD}, whereas values greater than one in panel a and below the 1:1 line in panel b indicate that the ΔP_{CD} was dominantly due to the trend of SM and VPD.

Owing to the underestimation of the SM-VPD coupling in the RCM models, the P_{CD} was also lower (2±0.7% and 3.6±2.1% during reference and present periods, respectively; Figure S11a) than what was calculated based on the in-situ and reanalysis data (E-OBS and ERA5-Land) with 3.5±0.7 % and 6.0±2.4% during reference and present period, respectively (Figure S5). However, the no significant change was observed in P_{CD} during the present period in comparison to the reference period, obtained by in-situ and reanalysis data (E-OBS and ERA5-Land), and the RCM ensembles i.e., 72% increase by the former dataset and 75% increase by latter dataset (Figure S11b). This pattern was also spatially consistent across different land cover types (Figures S11c).

For the future, the RCM ensembles showed a 3.4-fold [2.0,6.5] (median[10th percentile, 90th percentile]) increase in the frequency of compound extreme dryness across Europe during the mid 21st century (2030-2065 period) compared to reference period (Figure S11b) with the largest increase in MED, some parts of NEU (high latitudes of Norway, Sweden, and Finland) and the surrounding Alpine region in CEU (Figure 9a). All land cover types were projected to experience on average more than three times the frequency of compound extreme dryness by the mid 21st century as compared to the reference period, with the highest increase in frequency for open shrublands (Figure 9c). By the late 21st century, the projections indicated a further increase in the frequency of occurrence of compound extreme dryness of 4.2-fold [2.0,10.8] in comparison to the reference period (Figure S11b), with a spatial pattern rather similar to that of the mid 21st century (Figure 9b). Only the northern part of CEU (northern Germany and Poland) indicated a decreased frequency of compound extreme dryness during the late 21st century in comparison to mid 21st century, most likely due to an increase in SM_{10P} (Figure S8a). Among different land cover types, open shrublands, grasslands and broadleaved forests were projected to experience more than five times more frequent compound dryness extremes during the late 21st century than compared to late 20th century (Figure 9d). Finally, the increase in frequency of compound extreme dryness during mid 21st century and late 21st century compared to the reference period is entirely and dominantly driven by decreasing SM and/or increasing VPD trend from reference to future periods throughout Europe.

Discussion

Here we assessed frequency and intensity of extreme dryness across Europe at a higher spatio-temporal resolution (0.1° × 0.1°, and daily) than previous studies conducted based on GCM and ESM simulations of much coarser spatio-temporal resolution (e.g., 2.5° × 2.5°, and monthly)[12,29]. This higher resolution of our analysis enabled us to segregate the increase in extremes, across present land cover types and regions (e.g., Alpine, Mediterranean, Northern Europe) across Europe. Our study showed that large parts of Europe, especially Central and Mediterranean Europe, have been experiencing increasing trends in model-based soil moisture and observation-based atmospheric drying, thereby resulting in the development of compound dry conditions since 1950. We showed that compared to a reference period (1950-1990), the frequency of compound extreme dryness, extreme soil dryness and extreme air dryness across Europe during 1991 to 2021 increased by a median of 1.7-fold, 1.2-fold, and 1.6-fold, respectively, mostly over Central and Mediterranean Europe. Regional climate model simulations for Europe indicated a further 3.4-fold increase in the frequency of compound dry extremes during mid-century (2030-2065), and a 4.2-fold increase during the late 21st century (2066-2100) most pronounced over present day broadleaved forests, croplands, and grasslands. Furthermore, increase in present and future frequency of compound dry extremes was more due to an increase in extreme air dryness than in extreme soil dryness.

The lower RCM based increase in frequency and intensity of extreme soil dryness than that from ERA5-Land was probably due to a disagreement in SM depth i.e., surface SM (0-7 cm) from ERA-Land, whereas that from the RCM represents the soil moisture over the complete soil profile (depth varying from 2.7m to 3m), as surface and total soil moisture trends as simulated by RCMs could different[30].The changes in extreme air dryness (relative to the reference period) as simulated by the RCMs agreed well with the observations across Europe. The RCMs showed a weaker daily SM and VPD coupling than that from the reanalysis/observation datasets, contradicting the results[31,32] that suggested a stronger SM and VPD coupling than the observations in GCMs. However, the higher SM and VPD correlations from the reanalysis/observation datasets could be a result from the different soil depth considered, as fluctuations of top soil moisture is higher than a complete soil profile. Nevertheless, both RCM and reanalysis/observation data showed similar change in occurrence probability of compound extreme dryness (75% for the former and 72% for the latter) during the present period compared to reference period. This indicated that the potential bias (in absolute values) between the RCMs and the reanalysis/observation data seemed to have little effect on the relative change in SM and VPD coupling over time. This observation was similar to recent studies showing RCMs and observation based agreement on warming trends even though there is substantial air temperature bias between RCMs and observations[27,33].

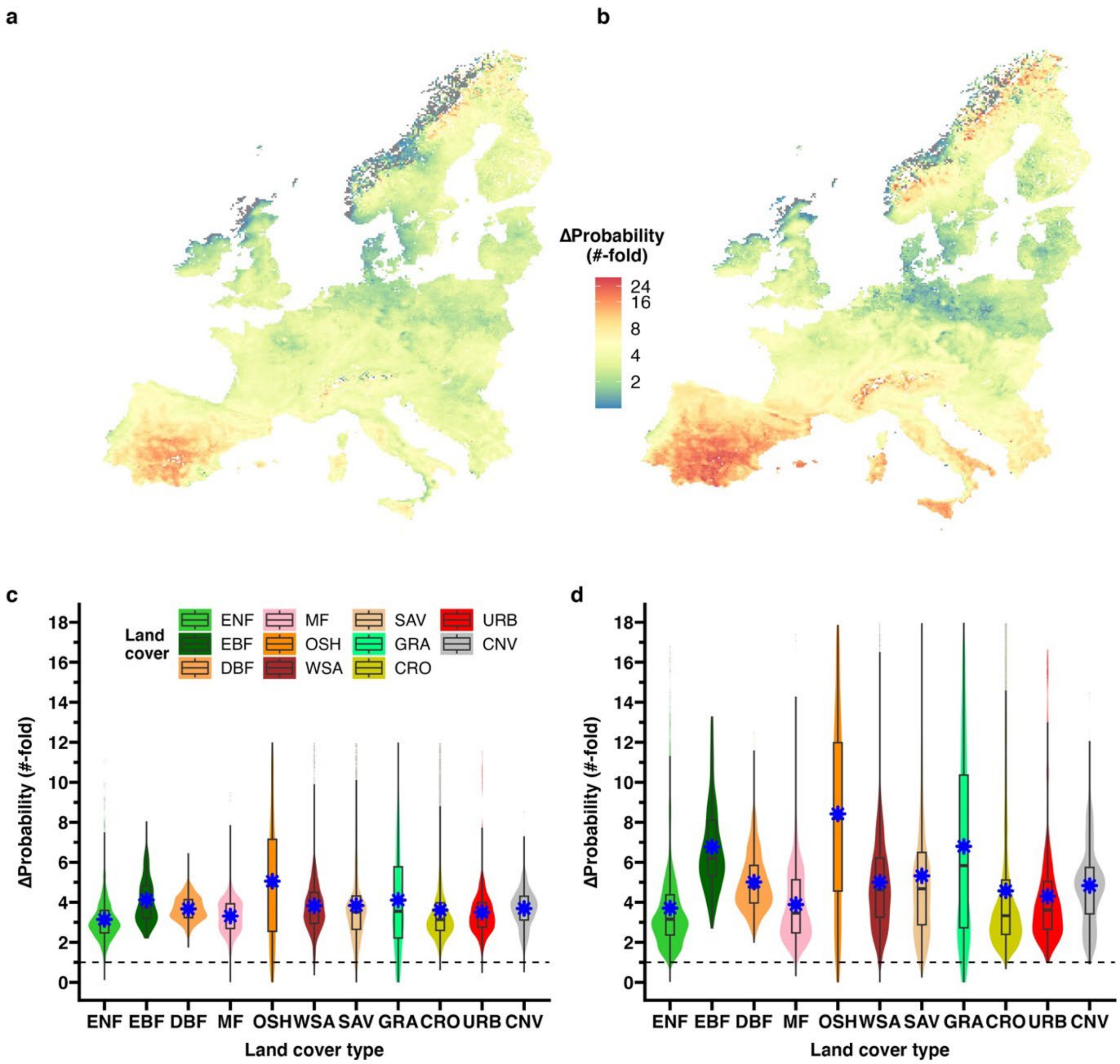

Figure 9. Change in probability of compound extreme dryness compared to the reference period (1950-1990) across Europe during **(a)** mid 21st century (2031-2065) and **(b)** late 21st century and across different land cover types during **(c)** mid 21st century and **(d)** late 21st century. The blue asterisk in panels c and d shows the means. The land cover types are based on the IGBP land cover classification (see Figure S1).

The increase in the frequency and intensity of compound dry extremes over time was generally due to two reasons, first due to an increased negative coupling between SM and VPD, and second due to an increasing trend of VPD and/or decreasing trend of SM, both signs of increasing dryness. The increase in the negative SM-VPD coupling (during 1991 to 2021 compared to the reference period) was a major reason of the increased frequency of compound extreme dryness across NEU, whereas the increased frequency of compound extreme dryness for much of CEU and MED was due to both above mentioned reasons but dominantly due to increasing trend of VPD and/or decreasing trend of SM. Such a SM-VPD coupling-driven increase and trend-driven increase in frequency of compound hot and drought events in Europe was also reported earlier[17,34]. However, we observed that much of the increased frequency and intensity of compound extreme dryness in future was due to increased air dryness across Europe. A Similar study[12] using GCM simulations, highlighted that the increase in frequency probability of compound extreme dryness (at a monthly timescale) was largely due to an increasing trend of VPD in the future.

The compound extreme dryness is a result of a series of complementary physical processes involving land-atmosphere feedbacks. High VPD-driven increases in ET reduces SM which then reduces ET and thus increases the sensible heat flux which warms and dries near-surface air, thereby increasing VPD, ultimately creating a positive feedback loop[19,35–39]. These feedback loops are much stronger over semi-arid regions than humid regions[36], which also explains the largest increase in the frequency of compound extreme in the present and the future over majority of Mediterranean Europe. Apart from these feedback loops, large-scale atmospheric anomalies such as blocking, subsidence, and free tropospheric warming had been identified as key contributors to the onset and continuation of extreme compound dry conditions[40,41]. These anomalies might also have contributed to the SM-VPD interaction.

The increasing trend in VPD was largely due to global warming driven-increase in air temperature, whereas soil drying trends could be due to increased ET trends in Europe with non-significant precipitation change over the last 40 years[9,13,40]. Furthermore, the future projections of intensifying VPD and drying SM along with the increase in negative coupling between SM-VPD could further increase the frequency and intensity of compound dry extremes in Europe. Owing to the direct role of SM and VPD on vegetation productivity, the future carbon uptake capacity could be highly compromised due to the rise in dry extremes in Europe. Although it is possible that future CO_2 fertilization effects (increased gross primary productivity due to more CO_2 rich atmosphere) could compensate for the loss in carbon uptake caused by compound extreme dryness[42], the

ESM (Earth System Models) forecasts showed that this was not the case for Central and Mediterranean Europe, but for Northern Europe[12], resulting in an unchanged future CO_2 uptake.

Conclusions

Our study detected extreme dryness across Europe at a higher spatio-temporal (0.1° and daily) resolution than previous studies which were conducted based on GCM and ESM simulations of much coarser resolution (e.g., 2.5° and monthly). At this higher resolution, we were able to segregate the changes in frequency of extreme dryness across the most recent (year 2021) land cover types in Europe, to quantify their present and future exposure to extreme dryness. This segregation is important for future climate mitigation planning and development of nature based solutions to our climate issues. Although almost all the land cover types were exposed to increased frequency of extreme dryness (all three types), croplands, broadleaved forest (EBF and DBF) and urban areas experienced more than twice as much extreme dryness conditions during 1990-2021 compared to reference period of 1990-2021. In the future, these land cover types would be exposed to more than three times as many extremes during mid-21st century compared to the 1950-1990 period. Such a high increase in extremes exposure will increase their vulnerability in the future, leading to a weaker terrestrial carbon sink and compromised food security across Europe. The prominent pattern of extreme dryness shown here is an essential first step in understanding how compound dryness has evolved over the years, and in developing new adaptive management policies to reduce the risks of upcoming hydroclimatic hazards.

Methods

Vapor pressure deficit and soil moisture data from 1950-2021

The study area is Europe (Latitude: 11°W - 33°E; Longitude: 35.8°N-72°N), comprising of three distinct regions[17], namely Northern Europe (NEU), Central Europe (CEU) and Mediterranean Europe (MED; Figure S1). We used the E-OBS v26.0e dataset [25,43] is a Europe-wide, observation-based, daily, gridded (0.1°x 0.1°) meteorological dataset covering 1950 to 2021 (72 years). We used daily average temperature (Tg; °C) and relative humidity (RH; %) data from E-OBS in this study. We calculated vapor pressure deficit (VPD, kPa) from mean temperature and relative humidity using equation 1[44].

$$VPD = \left(1 - \frac{RH}{100}\right) \times 0.6107 \times 10^{\frac{7.5 \times Tg}{237.3 + Tg}} \qquad (1)$$

We obtained the surface (0-7 cm depth) soil moisture (SM) data from the most recent reanalysis data from ECMWF's (European Centre for Medium-range Weather Forecasts) new land component of the fifth generation of European Reanalysis (ERA5-Land) dataset[26] spanning over seven decades (1950–2021). The ERA5-Land uses the Tiled ECMWF Scheme for Surface Exchanges over Land with a revised land surface hydrology (HTESSEL)[45]. The SM data from ERA5-Land is available at an hourly resolution with spatial resolution of 0.1° × 0.1°. We aggregated SM data from hourly values to daily means for our analysis. Recent in-situ and satellite based validation studies have shown high accuracy of surface SM simulation of ERA5-Land[26,46,47]. We obtained both the ERA5-Land and E-OBS datasets from the climate data store of Copernicus Climate Change Service (https://cds.climate.copernicus.eu). Additionally, we also obtained the land cover data for the year 2021 from MODIS product MCD12Q1 Version 6.1[28], which gives yearly land cover information at 500m resolution as per International Geosphere Biosphere Program (IGBP) classification: ENF – Evergreen needleleaf forest, EBF – Evergreen broadleaf forest, DBF – Deciduous broadleaf forest, MF – Mixed forest, OSH – Open shrublands, WSA – Wooden savannas, SAV – Savannas, GRA – Grasslands, CRO – Croplands, URB – Urban and built-up areas, CNV – Cropland and natural vegetations mosaics. In this study we masked out any barren land or water bodies. We then aggregated the land cover data to 0.1° × 0.1° resolution, by assigning the majority land cover types in each 0.1° × 0.1° grid.

Future projection data until 2100

We used the climatic projections of the EURO-CORDEX project (domain: EUR-11; http://www.euro-cordex.net) from 1950-2100 to project compound extreme dryness into the future. EURO-CORDEX is the European branch of the international CORDEX initiative, which is a program sponsored by the World Climate Research Program (WRCP) to organize an internationally coordinated framework to produce improved regional climate change projections for all land regions world-wide[27,48]. EURO-CORDEX project offers simulation of higher spatiotemporal resolution (daily at 0.11° × 0.11° resolution) that allow us to improve our understanding on past, present and future evolution of extreme events. We used daily means of surface air temperature (i.e., tas, K), surface relative humidity (i.e., hurs, %), and total soil moisture content (i.e., mrso, kg/m^2) from five regional climate models (RCMs), namely ALADIN63, HadREM3-GA7-05, RACMO22E, CCLM4-8-17, and HIRHAM5, using the boundary conditions from the MPI-M-MPI-ESM-LR global climate model driven under the RCP8.5 (Representative Concentration Pathways 8.5) emission scenario. The RCP8.5 based future projections is widely used in recent studies focusing on future evolution of extreme events[12,34,49,50]. We calculated the daily VPD for the future projection from surface air temperature and relative humidity using equation 1.

Statistical analyses

All statistical data analyses carried out in this study were performed in R statistical programming language[51] and involved the following steps:

1. Since dryness extremes are relevant for terrestrial carbon cycle, we focused all our analyses on the during April-September months (183 days) as most of the carbon sink activity occurs during this period across Europe (Peters et al., 2010). We assumed 1950-1990 as a reference period (total 41*183 = 7503 days) and 1991-2021 as the present period (total 5673 years). We divided the future period into two slices of 35 years each: 2031-2065 (mid 21st century; 6405 days) and 2066-2100 (late 21st century; 6405 days) to quantify and compare the frequency and intensity of each type of extremes (extreme soil dryness, extreme air dryness and compound extreme dryness). Initial data preprocessing (calculation and daily aggregation of VPD) was done using CDO (climatic data operators) software[52] and the '*raster*' R-package[53]
2. We detected trends (from 1950-2021) of yearly mean SM and VPD (mean SM and VPD of each year), and yearly 10th percentile SM (SM_{10P}; one for each year) and 90th percentile VPD (VPD_{90P}; one for each year) across Europe (i.e. for each 0.1° × 0.1° grid). The yearly trend was calculated by a modified Mann-Kendall trend test using

the ‘*rtrend*’ R-package, which accounts for the serial correlation in the time series data[54].

3. We used the “peak over threshold” approach to identify extreme soil dryness (SM < SM_{10P}; 10th percentile SM), extreme air dryness (VPD > VPD_{90P}; 90th percentile VPD) and compound extreme dryness days (SM < SM_{10P} AND VPD > VPD_{90P}) across Europe during each of the reference, present and future periods[4,12]. The intensity of extremes was defined by the extreme SM and VPD thresholds, i.e., SM_{10P} and VPD_{90P}, for reference, present and future periods. Decrease in SM_{10P} (across different periods) implied increased intensity of extreme soil dryness, whereas increase in VPD_{90P} implied increased intensity of extreme air dryness and vice-versa.
4. We used bivariate copula to model the dependence structure of SM and VPD and calculate the occurrence probability of compound extreme dryness. Bivariate copulas are widely used to model the dependence between two random variables (here SM and VPD) with different marginal distributions[55]. Based on our definition in step 3, the joint occurrence probability of compound extreme dryness (P_{CD}) is given by equation 2 for any time period (*tp*; reference, present, and future) with SM and VPD thresholds from any period (*th*; reference, present, and future).

$$P_{CD}[tp,th] = P(SM[tp] < SM_{10P}[th] \cap VPD[tp] > VPD_{90P}[th])$$
$$= P(SM[tp] < SM_{10P}[th]) - P(SM[tp] < SM_{10P}[th] \cap VPD[tp] \leq VPD_{90P}[th])$$
$$= P(SM[tp] < SM_{10P}[th]) - C_{tp}(SM_{10P}[th], VPD_{90P}[th]) \quad (2)$$

where, C_{tp} is the cumulative distribution function of the bivariate copula estimated on any period, tp. The detailed theory about bivariate copulas can be found in the literature[55,56]. Copula modeling was done for each grid for each different periods – e.g., for reference period we used SM and VPD data for 7503 days for each grid point to detect its SM_{10P} and VPD_{90P} to finally calculate P_{CD}. We considered commonly used copula families (Gaussian copula, Student’s t copula, and Archimedean copula) and used the best fit copula based on the Bayesian Information Criterion to calculate P_{CD}. The copula analysis was performed using the “*VineCopula*” R package[57], with which we used the function ‘*BiCopSelect*’ to select the best fit copula function and then used function '*BiCopCDF*' to calculate the P_{CD}. We also compared our P_{CD} obtained from the copula method with P_{CD} obtained from a simple counting method (fraction of days exceeding the SM and VPD thresholds). We found negligible differences between the two methods (maximum and mean absolute differences of 2.1% and 0.05%, respectively). Such negligible differences were expected as we are analyzing daily data with little data limitation (> 5000 days for each grid during reference, present and future periods). In this study, we describe all our P_{CD} based on the copula method as estimated with equation 2.

5. We calculated the probability multiplication factor (PMF) across Europe for different periods (reference, present and future) to quantify the change in occurrence probability of compound extreme dryness due to covariance of SM and VPD[19]. PMF of any period is the ratio of P_{CD} (joint probability calculated by bivariate copula with thresholds of the corresponding periods) and 0.01 (assuming SM and VPD are independent = $0.1 \times 0.1 = 0.01$). Therefore, a value of PMF = 1 implies that there was no change in occurrence probability due to covariance of SM and VPD. PMF for any period (*tp*) was calculated as shown by equation 3.

$$PMF\,[tp] = \frac{P_{CD}[tp, th]}{0.01};\ th = tp = reference, present\ \&\ future \qquad (3)$$

where both *tp* and *th* are of the same period.

6. Finally, to quantify changes in the occurrence probability of compound extreme dryness (ΔP_{CD}) in present and future periods (*tp* = present & future) relative to the reference period (*th* = reference), we used the extreme thresholds (SM_{10P} and VPD_{90P}) of the reference period to calculate P_{CD} (as per equation 2), i.e., *th* = reference period, during the present period (1991-2021; tp = present) and two future periods (*tp* = mid 21st century and late 21st century) for E-OBS and ERA5-Land data (present period) each RCM model (for present and future comparisons) as shown in equation 4.

$$\Delta P_{CD}[tp] = \frac{P_{CD}[tp, reference]}{P_{CD}[reference, reference]}; tp = present\ \&\ future \qquad (4)$$

The ΔP_{CD} for any period present and future period (*tp*) can be segregated into ΔP_{CD} due to changes in SM-VPD coupling (ΔP_{CD} coupling) and changes in SM and/or VPD trend (ΔP_{CD} trend) as shown in equations 5 and 6.

$$\Delta P_{CD} coupling\ [tp] = \frac{PMF\ [tp]}{PMF\ [reference]}; tp = present\ \&\ future \quad (5)$$

$$\Delta P_{CD} trend\ [tp] = \frac{P_{CD}[tp, reference]}{0.01 \times PMF\ [tp]}; tp = present\ \&\ future \quad (6)$$

Final present and future occurrence probability from all five RCM models were averaged to calculate the average change in probability of compound extreme dryness in present and future periods. We further performed the analysis from Step 1 to Step 5 at a monthly scale with mean monthly VPD and SM to compare the PMF from two different

Data and Code availability

All data used in this study is openly available in the following database. The E-OBS and ERA5-Land datasets were downloaded from the climate data store of Copernicus Climate Change Service (https://cds.climate.copernicus.eu). The 2021 MODIS land cover product MCD12Q1 Version 6.1 was downloaded from USGS LP DAAC website https://lpdaac.usgs.gov/products/mcd12c1v061/. The EURO-CORDEX simulations were downloaded from ESGF data node https://esgf-data.dkrz.de/search/cordex-dkrz/. All data and R script used to construct the visuals in the manuscript can be requested from the corresponding author.

References

1. Yin, D., Roderick, M. L., Leech, G., Sun, F. & Huang, Y. The contribution of reduction in evaporative cooling to higher surface air temperatures during drought. *Geophysical Research Letters* **41**, 7891–7897 (2014).

2. Teuling, A. J. A hot future for European droughts. *Nature Clim Change* **8**, 364–365 (2018).

3. Seneviratne, S. *et al.* Changes in climate extremes and their impacts on the natural physical environment. *Intergovernmental Panel on Climate Change (IPCC)* 109–230 (2012) doi:10.7916/d8-6nbt-s431.

4. Zscheischler, J. & Seneviratne, S. I. Dependence of drivers affects risks associated with compound events. *Science Advances* **3**, (2017).

5. Liu, L. *et al.* Soil moisture dominates dryness stress on ecosystem production globally. *Nature Communications* **11**, 4892 (2020).

6. Humphrey, V. *et al.* Soil moisture-atmosphere feedback dominates land carbon uptake variability. *Nature* **592**, 65–69 (2021).

7. Yuan, W. *et al.* Increased atmospheric vapor pressure deficit reduces global vegetation growth. *Science Advances* **5**, (2019).

8. Fu, Z. *et al.* Atmospheric dryness reduces photosynthesis along a large range of soil water deficits. *Nature Communications 2022 13:1* **13**, 1–10 (2022).

9. He, B. *et al.* Worldwide impacts of atmospheric vapor pressure deficit on the interannual variability of terrestrial carbon sinks. *National Science Review* **9**, (2022).

10. Anderegg, W. R. L. Spatial and temporal variation in plant hydraulic traits and their relevance for climate change impacts on vegetation. *New Phytologist* **205**, 1008–1014 (2015).

11. Gharun, M. *et al.* Physiological response of Swiss ecosystems to 2018 drought across plant types and elevation. *Philosophical Transactions of the Royal Society B: Biological Sciences* **375**, 20190521 (2020).

12. Zhou, S., Zhang, Y., Park Williams, A. & Gentine, P. Projected increases in intensity, frequency, and terrestrial carbon costs of compound drought and aridity events. *Science Advances* **5**, eaau5740 (2019).

13. Lal, P., Shekhar, A., Gharun, M. & Das, N. N. Spatiotemporal evolution of global long-term patterns of soil moisture. *Science of The Total Environment* **867**, 161470 (2023).

14. Bastos, A. *et al.* Vulnerability of European ecosystems to two compound dry and hot summers in 2018 and 2019. *Earth System Dynamics* **12**, 1015–1035 (2021).

15. Hermann, M. *et al.* Meteorological history of low-forest-greenness events in Europe in 2002–2022. *Biogeosciences* **20**, 1155–1180 (2023).

16. Ionita, M. *et al.* The European 2015 drought from a climatological perspective. *Hydrology and Earth System Sciences* **21**, 1397–1419 (2017).

17. Markonis, Y. *et al.* The rise of compound warm-season droughts in Europe. *Science Advances* **7**, (2021).

18. Peters, W. *et al.* Seven years of recent European net terrestrial carbon dioxide exchange constrained by atmospheric observations. *Global Change Biology* **16**, 1317–1337 (2010).

19. Zhou, S. *et al.* Land–atmosphere feedbacks exacerbate concurrent soil drought and atmospheric aridity. *Proceedings of the National Academy of Sciences of the United States of America* **116**, 18848–18853 (2019).

20. Tatarinov, F. *et al.* Resilience to seasonal heat wave episodes in a Mediterranean pine forest. *New Phytologist* **210**, 485–496 (2016).

21. Stoy, P. C. *et al.* Biosphere-atmosphere exchange of CO_2 in relation to climate: a cross-biome analysis across multiple time scales. *Biogeosciences* **6**, 2297–2312 (2009).

22. Yuan, W. *et al.* Severe summer heatwave and drought strongly reduced carbon uptake in Southern China. *Sci Rep* **6**, 18813 (2016).

23. Geddes, J. A., Murphy, J. G., Schurman, J., Petroff, A. & Thomas, S. C. Net ecosystem exchange of an uneven-aged managed forest in central Ontario, and the impact of a spring heat wave event. *Agricultural and Forest Meteorology* **198–199**, 105–115 (2014).

24. Zweifel, R. *et al.* Why trees grow at night. *New Phytologist* **231**, 2174–2185 (2021).

25. Cornes, R. C., van der Schrier, G., van den Besselaar, E. J. M. & Jones, P. D. An Ensemble Version of the E-OBS Temperature and Precipitation Data Sets. *Journal of Geophysical Research: Atmospheres* **123**, 9391–9409 (2018).

26. Muñoz-Sabater, J. *et al.* ERA5-Land: A state-of-the-art global reanalysis dataset for land applications. *Earth System Science Data* **13**, 4349–4383 (2021).

27. Kotlarski, S. *et al.* Regional climate modeling on European scales: a joint standard evaluation of the EURO-CORDEX RCM ensemble. *Geoscientific Model Development* **7**, 1297–1333 (2014).

28. Friedl, M. & Sulla-Menashe, D. MCD12C1 MODIS/Terra+ Aqua Land Cover Type Yearly L3 Global 0.05 Deg CMG V006 [Data set]. *NASA EOSDIS Land Processes DAAC* (2015) doi:https://doi.org/10.5067/MODIS/MCD12C1.006.

29. Jha, S., Gudmundsson, L. & Seneviratne, S. I. Partitioning the Uncertainties in Compound Hot and Dry Precipitation, Soil Moisture, and Runoff Extremes Projections in CMIP6. *Earth's Future* **11**, e2022EF003315 (2023).

30. Berg, A., Sheffield, J. & Milly, P. C. D. Divergent surface and total soil moisture projections under global warming. *Geophysical Research Letters* **44**, 236–244 (2017).

31. Ukkola, A. M. *et al.* Land surface models systematically overestimate the intensity, duration and magnitude of seasonal-scale evaporative droughts. *Environ. Res. Lett.* **11**, 104012 (2016).

32. Levine, P. A., Randerson, J. T., Swenson, S. C. & Lawrence, D. M. Evaluating the strength of the land–atmosphere moisture feedback in Earth system models using satellite observations. *Hydrology and Earth System Sciences* **20**, 4837–4856 (2016).

33. van der Wiel, K., Selten, F. M., Bintanja, R., Blackport, R. & Screen, J. A. Ensemble climate-impact modelling: extreme impacts from moderate meteorological conditions. *Environmental Research Letters* **15**, 034050 (2020).

34. Cardell, M. F., Amengual, A., Romero, R. & Ramis, C. Future extremes of temperature and precipitation in Europe derived from a combination of dynamical and statistical approaches. *International Journal of Climatology* **40**, 4800–4827 (2020).

35. Gentine, P., Holtslag, A. A. M., D'Andrea, F. & Ek, M. Surface and Atmospheric Controls on the Onset of Moist Convection over Land. *Journal of Hydrometeorology* **14**, 1443–1462 (2013).

36. Miralles, D. G., Gentine, P., Seneviratne, S. I. & Teuling, A. J. Land–atmospheric feedbacks during droughts and heatwaves: state of the science and current challenges. *Annals of the New York Academy of Sciences* **1436**, 19–35 (2019).

37. Seneviratne, S. I. *et al.* Impact of soil moisture-climate feedbacks on CMIP5 projections: First results from the GLACE-CMIP5 experiment. *Geophysical Research Letters* **40**, 5212–5217 (2013).

38. Sippel, S. *et al.* Drought, Heat, and the Carbon Cycle: a Review. *Current Climate Change Reports* **4**, 266–286 (2018).

39. Shekhar, A., Hörtnagl, L., Buchmann, N. & Gharun, M. Long-term changes in forest response to extreme atmospheric dryness. *Global Change Biology* **n/a**, 1–18 (2023).

40. Fang, Z., Zhang, W., Brandt, M., Abdi, A. M. & Fensholt, R. Globally Increasing Atmospheric Aridity Over the 21st Century. *Earth's Future* **10**, e2022EF003019 (2022).

41. Pfahl, S., Schwierz, C., Croci-Maspoli, M., Grams, C. M. & Wernli, H. Importance of latent heat release in ascending air streams for atmospheric blocking. *Nature Geosci* **8**, 610–614 (2015).

42. Campbell, J. E. *et al.* Large historical growth in global terrestrial gross primary production. *Nature* **544**, 84–87 (2017).

43. Klein Tank, A. M. G. *et al.* Daily dataset of 20th-century surface air temperature and precipitation series for the European Climate Assessment. *International Journal of Climatology* **22**, 1441–1453 (2002).

44. Jones, Hamlyn G. *Plants and Microclimate: A Quantitative Approach to Environmental Plant Physiology*. (Cambridge University Press, 2014).

45. Hersbach, H. *et al.* The ERA5 global reanalysis. *Quarterly Journal of the Royal Meteorological Society* **146**, 1999–2049 (2020).

46. Albergel, C., De Rosnay, P., Balsamo, G., Isaksen, L. & Muñoz-Sabater, J. Soil moisture analyses at ECMWF: Evaluation using global ground-based in situ observations. *Journal of Hydrometeorology* **13**, 1442–1460 (2012).

47. Lal, P., Singh, G., Das, N. N., Colliander, A. & Entekhabi, D. Assessment of ERA5-Land Volumetric Soil Water Layer Product Using In Situ and SMAP Soil Moisture Observations. *IEEE Geoscience and Remote Sensing Letters* **19**, 1–5 (2022).

48. Vautard, R. *et al.* Evaluation of the Large EURO-CORDEX Regional Climate Model Ensemble. *Journal of Geophysical Research: Atmospheres* **126**, e2019JD032344 (2021).

49. Molina, M. O., Sánchez, E. & Gutiérrez, C. Future heat waves over the Mediterranean from an Euro-CORDEX regional climate model ensemble. *Sci Rep* **10**, 8801 (2020).

50. Schwalm, C. R., Glendon, S. & Duffy, P. B. RCP8.5 tracks cumulative CO2 emissions. *Proceedings of the National Academy of Sciences* **117**, 19656–19657 (2020).

51. R Core Team. R core team (2021). *R: A language and environment for statistical computing. R Foundation for Statistical Computing, Vienna, Austria. URL http://www. R-project. org* (2021).

52. Schulzweida, U. CDO User Guide. (2022).

53. Hijmans, R. J. *et al.* Package 'raster'. *R* (2014).

54. Kong, D. & Song, H. rtrend: Trend Estimating Tools. *R package version 0.1.3* (2022).

55. Genest, C. & Favre, A.-C. Everything You Always Wanted to Know about Copula Modeling but Were Afraid to Ask. *Journal of Hydrologic Engineering* **12**, 347–368 (2007).

56. Wable, P. S. & Jha, M. K. Application of Archimedean copulas to the impact assessment of hydro-climatic variables in semi-arid aquifers of western India. *Hydrogeology Journal* **26**, 89–108 (2018).

57. Nagler, T. *et al.* VineCopula: Statistical Inference of Vine Copulas. (2022).

Supplementary Files

This is a list of supplementary files associated with this preprint. Click to download.

- EuropeandrynessSINPJ.docx